Visualizing the Role of Bi 6s "Lone Pairs" in the Off-Center Distortion in Ferromagnetic $BiMnO_3$

Ram Seshadri[†] and Nicola A. Hill*[,‡]

Solid State and Structural Chemistry Unit, Indian Institute of Science, Bangalore 560 012, India, and Materials Department, University of California, Santa Barbara, California 93106-5050

Received February 2, 2001. Revised Manuscript Received June 5, 2001

Results of first-principles electronic structure calculations on the low-temperature monoclinic phase of the ferromagnetic perovskite $BiMnO_3$ [Atou et al. *J. Solid State Chem.* **1999**, *145*, 639] are presented. In agreement with experiments, the calculations obtain an insulating ferromagnetic ground state for this material. The role of Bi 6s "lone pairs" in stabilizing the highly distorted perovskite structure is examined using real-space visualization of the electronic structure. Comparisons are drawn with the electronic structures of hypothetical cubic $BiMnO_3$ and with the electronic structure of the prototypical perovskite manganite, $LaMnO_3$. The exploitation of s electron lone pairs in the design of new ferroic materials is suggested.

Introduction

$BiMnO_3$ crystallizes at high pressure in a highly distorted perovskite structure, which is both ferromagnetic and insulating. Ferromagnetic insulators are unusual; another example is $SeCuO_3$, which is also a highly distorted perovskite.[1,2] By contrast, $LaMnO_3$ and all the rare earth perovskite manganites are antiferromagnetic insulators, as expected from the usual superexchange argument.[3] This difference in behavior is particularly surprising in light of the similarity in ionic radii of La^{3+} and Bi^{3+}, which are, respectively, 1.216 and 1.24 Å (in nine-coordination).[4]

In addition to its fundamental interest as a ferromagnetic insulator, it has also been suggested that $BiMnO_3$ is ferroelectric.[5,6] Ferroelectricity and magnetism are rarely found in the same system because the off-center distortion responsible for polar behavior is usually incompatible with the partially filled d-levels which are a prerequisite for a magnetic ground state.[7,8]

The valence electron configuration of Bi is $6s^26p^3$. Therefore, the formally trivalent Bi in $BiMnO_3$ contains a lone pair of 6s electrons. The goal of our work in this paper is to investigate the role of the lone pair on Bi in both stabilizing the ferromagnetism and inducing the ferroelectric distortion. Such $6s^2$ lone pairs are often quite active from a structural viewpoint, resulting in distorted coordination polyhedra around the $6s^2$ species. The distorted monoclinic structure of $BiMnO_3$[9] has in fact been ascribed by Atou et al.[9] to the ordering of the Bi 6s lone pair. The $6s^2$ lone pair has also been indirectly implicated in the ferroelectric properties of systems such as $PbTiO_3$ whose behavior is rather different from ferroelectric $BaTiO_3$, a compound that is otherwise isoelectronic and nearly isostructural.[10] Likewise, the structural effects of lone pairs are well studied in PbO and related systems.[11,12] Recently, the role of the lone pair in driving the antiferroelectric transition in an ordered double perovskite Pb_2MgWO_6 has been suggested.[13]

In this paper, we elucidate the role of the $6s^2$ lone pair in $BiMnO_3$ by calculating the first principles electronic structure of monoclinic $BiMnO_3$ and comparing it with that of the undistorted cubic perovskite phase. We also compare the electronic structure of $BiMnO_3$ with that of $LaMnO_3$, in which no lone pair is present. In particular, we examine the effects of metal−oxygen covalency in both compounds and present a real space depiction of the stereochemistry of the lone pair in monoclinic $BiMnO_3$. We conclude that the lone pair drives the off-center distortion in monoclinic $BiMnO_3$ resulting in its novel multiferroic properties.

Computational Details

All calculations were performed on AMD Athlon PCs using density functional theory (DFT)[14] within the linear muffin tin orbital (LMTO) approximation. Total

* To whom correspondence should be addressed. Materials Department, University of California, Santa Barbara, CA 93106-5050, USA. Tel: (805) 893-7920. Fax: (805) 893-7221. E-mail: nahill@mrl.ucsb.edu.

[†] Solid State and Structural Chemistry Unit, Indian Institute of Science, Bangalore 560 012, India. Tel: 91 (80) 309-2952. Fax: 91 (80) 360-1310. E-mail: seshadri@sscu.iisc.ernet.in.

[‡] University of California.

(1) Kohn, K.; Horie, O.; Akimoto, S.-I.; Inoue, K. *J. Solid State Chem.* **1976**, *18*, 27.

(2) Subramanian, M. A.; Ramirez, A. P.; Marshall, W. *J. Phys. Rev. Lett.* **1999**, *82*, 1558.

(3) Rao, C. N. R.; Cheetham, A. K.; Mahesh, R. *Chem. Mater.* **1996**, *8*, 2421.

(4) Shannon, R. D.; Prewitt, C. T. *Acta Crystallogr. B* **1969**, *25*, 925; Shannon, R. D. *Acta Crystallogr. A* **1976**, *32*, 751.

(5) Hill, N. A.; Rabe, K. M. *Phys. Rev. B* **1999**, *59*, 8759.

(6) Santos, A. M.; Raju, A. R.; Parashar, S.; Cheetham, A. K.; Rao, C. N. R., private communication.

(7) Hill, N. A. *J. Phys. Chem. B* **2000**, *104*, 6694.

(8) Filippetti, A.; Hill, N. A. *Phys. Rev. B*, submitted for publication.

(9) Atou, T.; Chiba, H.; Ohoyama, K.; Yamaguchi, Y.; Syono, Y. *J. Solid State Chem.* **1999**, *145*, 639.

(10) Cohen, R. E. *Nature* **1992**, *358*, 136.

(11) Trinquier, G.; Hoffmann, R. *J. Phys. Chem.* **1984**, *88*, 6696.

(12) Watson, G. W.; Parker, S. C. *J. Phys. Chem. B* **1999**, *103*, 1258; Watson, G. W.; Parker, S. C.; Kresse, G. *Phys. Rev. B* **1999**, *59*, 8481.

(13) Seshadri, R.; Baldinozzi, G.; Felser, C.; Tremel, W. *J. Mater. Chem.* **1999**, *9*, 2463.

(14) Hohenberg, H.; Kohn, W. *Phys. Rev.* **1964**, *136*, 864; Kohn, W.; Sham, L. *J. Phys. Rev.* **1965**, *140*, 1133.

10.1021/cm010090m CCC: $20.00
Published on Web 08/11/2001

energies, densities of states and electron densities were calculated using the scalar-relativistic linear muffin-tin orbital method[15] in the atomic sphere approximation (ASA) as implemented in version 47 of the Stuttgart TB-LMTO-ASA program.[16] A detailed description of the LMTO-ASA method, including its applications, can be found elsewhere.[17] In these calculations, the partitioning of space into atom-centered and empty spheres is done through an automatic procedure which ensures that overlap between atomic spheres does not exceed 16%. For the empty spheres, 1s orbital bases were used, and the 2p orbital was dealt with through the downfolding technique. The basis sets for the atomic spheres were 6s and 6p for Bi with 6d and 5f downfolded; 4s, 4p, and 3d for Mn with 4f downfolded, and 2p orbitals on O with 3s and 3d downfolded. Scalar-relativistic Kohn−Sham equations were solved taking all relativistic effects into account except for the spin−orbit coupling. Spin-polarization was achieved within the nonlocal Perdew−Wang exchange correlation formalism.[18] For the monoclinic structure of $BiMnO_3$, 78 irreducible k points in the primitive wedge of the Brillouin zone were used while for the cubic structure, 84 irreducible k points were used.

The present LMTO method makes use of atom-centered spheres and empty spheres between atoms. Any structural change requires a completely new set of atomic and empty spheres, so this method is not of use for examining the energetics of structural change, for example, by attempting to relax the structure to a ground state. We have made no attempt to do so.

The LMTO electronic structures were analyzed by calculating crystal orbital Hamiltonian populations (COHPs) and electron localization functions (ELFs). The crystal orbital Hamiltonian population COHP[19] is the density of states weighted by the corresponding Hamiltonian matrix element and is indicative of the strength and nature of a bonding (positive COHP) or antibonding (negative COHP) interaction. COHPs are similar to the crystal orbital overlap populations (COOPs) introduced by Hoffmann and co-workers.[20] The ELFs (introduced by Becke and Edgecombe) facilitate visualization of the bonding and the lone pairs in real space.[21,22] Following Silvi and Savin,[22] the ELF is defined as:

$$\mathrm{ELF} = [1 + (D/D_h)^2]^{-1}$$

where

$$D = \frac{1}{2}\sum_i |\nabla\phi_i|^2 - \frac{1}{8}\frac{|\nabla\rho|^2}{\rho} \text{ and } D_h = \frac{3}{10}(3\pi^2)^{5/3}\rho^{5/3}$$

Here ρ is the electron density, and ϕ_i are the Kohn−Sham wave functions. The electron localization function provides a measure of the local influence of Pauli repulsion on the behavior of electrons and permits the mapping in real space of core, bonding, and nonbonding regions in a crystal.[22] Of relevance to this work is the previous use of ELFs to visualize bonding in solids formed from the carbon group elements.[23]

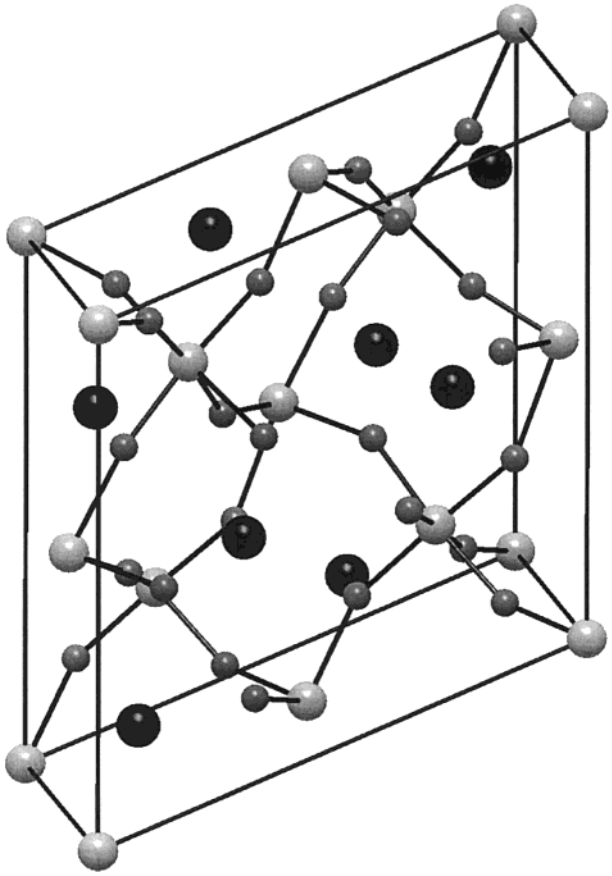

Figure 1. Crystal structure of monoclinic $BiMnO_3$ projected nearly down the b axis. The large black spheres are Bi, and the smaller white spheres are Mn, six-coordinate with oxygen.

We have made no attempt to obtain the ground-state structure. Instead, crystal structure data were taken from the neutron/electron diffraction study of Atou et al.[9] The unit cell volume is ≈493 Å^3, and there are 10 atoms in the asymmetric unit. We display the crystal structure of monoclinic (space group C2) $BiMnO_3$ in Figure 1 showing a view down the b-axis of the structure. Note the highly Jahn−Teller elongated MnO_6 octahedra. As many as 17 empty spheres in the asymmetric unit were required for space filling in this structure. The ideal ABO_3 cubic perovskite structure, in which the small (B) cation is surrounded by an octahedron of oxygen anions, with large (A) cations at the unit cell corners, is shown in Figure 2. For calculations on the cubic phases of perovskite $LaMnO_3$ and $BiMnO_3$, a cell parameter of 3.95 Å was chosen based on the average experimental $LaMnO_3$ bond lengths.[5] Calculations were also performed for A-type antiferromagnetic $LaMnO_3$ using the 14 K orthorhombic structure reported by Huang et al.[24] with 80 irreducible k points in the primitive wedge of the BZ.

(15) Andersen, O. K. *Phys. Rev. B* **1975**, *12*, 3060; Jepsen, O.; Andersen, O. K. *Z. Phys. B* **1995**, *97*, 35.
(16) Tank, R. W.; Jepsen, O.; Burkhardt, A.; Andersen, O. K. *The Stuttgart TB-LMTO-ASA Program*, version 47; MPI für Festkörperforschung: Stuttgart, Germany, 1998.
(17) Skriver, H. L. *The LMTO Method*; Springer: Berlin, 1984.
(18) Perdew, J. P.; Wang, Y. *Phys. Rev. B* **1986**, *33*, 8800; Perdew, J. P.; Chevary, J. A.; Vosko, S. H.; Jackson, K. A.; Pederson, M. R.; Singh, D. J.; Fiolhais, C. *Phys. Rev. B* **1992**, *46*, 6671.
(19) Dronskowski, R.; Blöchl, P. E. *J. Phys. Chem.* **1993**, *97*, 8617; Boucher, F.; Rousseau, R. *Inorg. Chem.* **1998**, *37*, 2351.
(20) Wijeyesekera, S.; Hoffmann, R. *Organomet.* **1984**, *3*, 949.
(21) Becke, A. D.; Edgecombe, K. E. *J. Chem. Phys.* **1990**, *92*, 53.
(22) Silvi, B.; Savin, A. *Nature* **1994**, *371*, 683.
(23) Savin, A.; Jepsen, O.; Andersen, O. K.; Preuss, H.; von Schnering, H. G., Angew. Chemie. **1992**, *104*, 185; *Angew. Chem., Intl. Ed. Engl.* **1992**, *31*, 187.

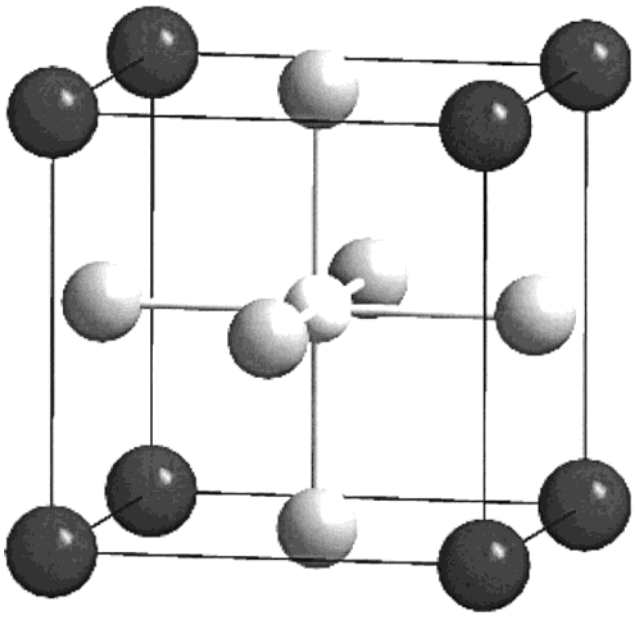

Figure 2. The ideal cubic perovskite structure. The small B cation (in white) is at the center of an octahedron of oxygen anions. The large A cations (black) occupy the unit cell corners.

Table 1. Relative Energies of Different Magnetic Phases in Cubic Paramagnetic $BiMnO_3$ and $LaMnO_3$

	$BiMnO_3$	$LaMnO_3$
FM	0	0
A-AFM	+88 meV	+110 meV
G-AFM	+435 meV	+365 meV
PM	+1.25 eV	+1.16 eV

Results

3.1 Cubic $BiMnO_3$ and Cubic $LaMnO_3$. First, we compare the properties of different magnetic phases of both $BiMnO_3$ and $LaMnO_3$ in the ideal cubic structure. Table 1 shows the relative energies of the paramagnetic (PM), ferromagnetic (FM), and A-type and G-type antiferromagnetic (AFM) phases of cubic $BiMnO_3$ and $LaMnO_3$. The A-type AFM phase consists of ferromagnetically aligned (100) planes of Mn ions coupled antiferromagnetically to each other, whereas in the G-type AFM structure each Mn ion is surrounded by six antiferromagnetically coupled neighbors. All values were calculated at the same lattice constant of 3.95 Å. The relative energies of FM and AFM phases of $LaMnO_3$ are taken from ref 25. Those for $BiMnO_3$ are calculated in this work using the LMTO method described above and a plane wave pseudopotential method[26] for the cubic phases to confirm the accuracy. The most striking feature is that in both cases the ferromagnetically ordered state is the most stable phase. This has been pointed out previously for $LaMnO_3$,[25] and the relationship between the observed Jahn−Teller distortion and the resulting A-type antiferromagnetic ground state is well understood.[27] The relative orderings of the states is the same in $BiMnO_3$ as in $LaMnO_3$, with the G-type AFM state being considerably less stable than the A-type and the nonmagnetic state being around 1 eV higher in energy than any of the spin-polarized phases. Also, in both cases the calculated magnetic moment is about 3.4 μ_B per Mn for the cubic FM and AFM structures. This is slightly lower than the spin-only value of 4 μ_B for the Mn^{3+} ion because of covalent bonding between the Mn 3d and O 2p electrons.

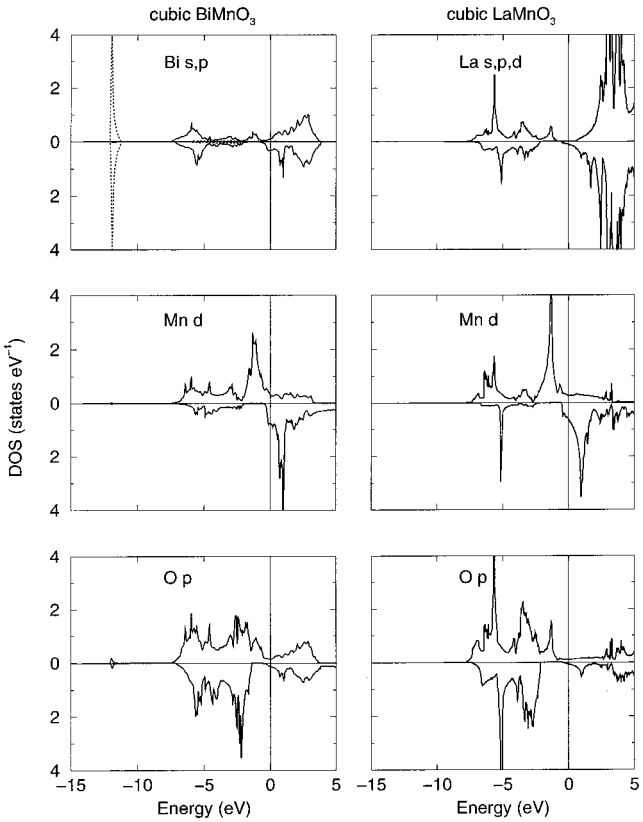

Figure 3. Projected DOS of the cubic forms of ferromagnetic $BiMnO_3$ and ferromagnetic $LaMnO_3$. The upper panel in each plot corresponds to majority (up) spin states, and the lower panel corresponds to minority (down) spin states.

These similarities in the magnetic properties of the cubic phases imply that the differences in magnetic properties in the low-temperature phases of $BiMnO_3$ and $LaMnO_3$ are caused entirely by the different geometries. Next we compare the calculated electronic properties of the cubic phases to investigate whether the driving force for the different structural distortions is already apparent in the high-symmetry structures.

Figure 3 compares the orbital-resolved densities of states (DOSs) of cubic ferromagnetic $BiMnO_3$ and $LaMnO_3$. (The total densities of states of cubic para- and ferromagnetic $LaMnO_3$ and $BiMnO_3$ have been compared previously and therefore are not shown here.[5]) Both materials are metallic in the cubic phase. The Mn and O states in the two compounds are similar in extent and even in the nature of the spin polarization. In both cases, the density of states shows a broad band composed largely of O 2p and Mn 3d orbitals ranging from around 7.5 eV below the Fermi level to around 5 eV above it. The Mn states occupy the same energy range as the oxygen states, suggesting a significant Mn−O covalency (confirmed by calculation of the COHPs). The exchange splitting between the majority and minority Mn 3d bands can be seen clearly, with the majority (up-spin say) bands largely filled and the minority (down-

(24) Huang, Q.; Santoro, A.; Lynn, J. W.; Erwin, R. W.; Borchers, J. A.; Peng, J. L.; Greene, R. L. *Phys. Rev. B* **1997**, *55*, 14987.
(25) Pickett, W. E.; Singh, D. J. *Phys. Rev. B* **1996**, *53*, 1146.
(26) The ABINIT code is a common project of the Universite Catholique de Louvain, Corning Incorporated, and other contributors (URL http://www.pcpm.ucl.ac.be/abinit).
(27) Goodenough, J. B. *Phys. Rev*. **1955**, *100*, 564.

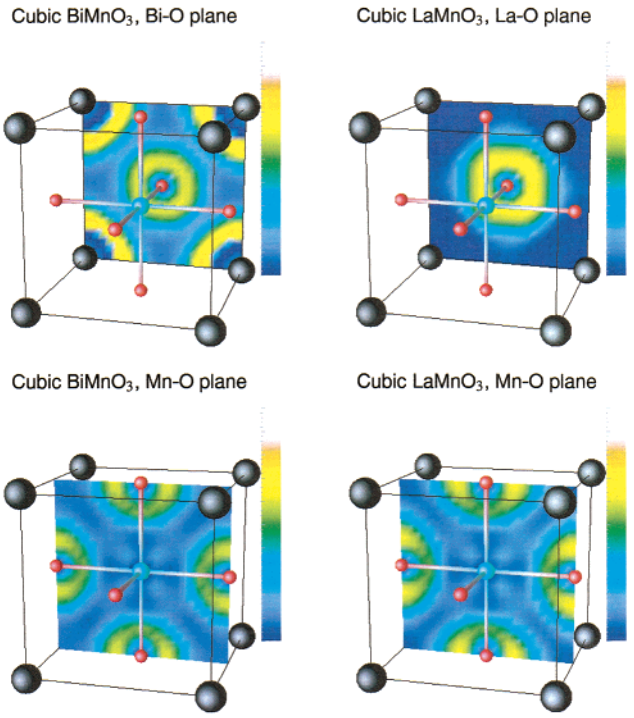

Figure 4. Valence ELFs projected onto different planes in the cubic structures of $BiMnO_3$ and $LaMnO_3$. The blue end of the scale bar corresponds to almost no electron localization, and the white end corresponds to complete localization. In these structural representations, the perovskite A atom (Bi or La) is in the corner of the cell and the B atom (Mn) is at the center, six-coordinate with O.

spin) largely unoccupied. The most obvious *difference* in the densities of states of the two compounds is the presence of the filled 6s levels on Bi, indicated by dotted lines. There is also a significant density of Bi 6p states below the Fermi level and in the same energy range as the O 2p states, providing the possibility for Bi−O hybridization. (The surprising presence of filled La states below E_F in cubic $LaMnO_3$ is an artifact, arising from the very large La sphere necessitated by the unphysical 12-coordination in cubic $LaMnO_3$. Also there are narrow peaks in the O states that are reflected in Mn as well as in La states. These narrow peaks arise once again due to the unphysical structure of cubic $LaMnO_3$.)

In Figure 4, the ELFs projected onto the A−O and Mn−O planes are displayed. Here the Mn is at the center of the unit cell and the large cations are at the corners. The color scheme is shown in the bar accompanying the images, with deep blue signifying one extreme of almost no localization (nearly-free electrons) and white signifying regions where electrons are completely localized. The ELFs in the Mn−O plane are very similar for the two compounds However, large differences can be seen in the A−O plane. The 6s "lone pairs" on Bi are approximately spherically distributed around the Bi atoms forming orange rings of localization. It has been pointed out previously that spherically distributed lone pairs tend to be unstable and the tendency of the lone pair to localize into a lobe shape can be strong enough to drive a structural distortion.[13] In contrast, the ELF around the La atoms in $LaMnO_3$ indicates almost zero electron localization.

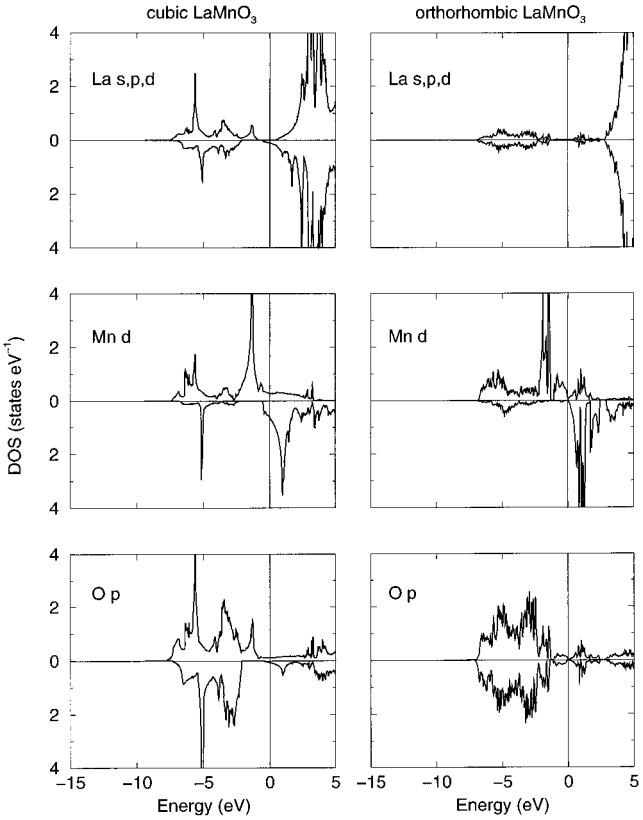

Figure 5. Projected DOS of cubic ferromagnetic $LaMnO_3$ as compared with the projected DOS of orthorhombic antiferromagnetic (A-type) $LaMnO_3$. The DOS of the latter have been scaled to one $LaMnO_3$ formula unit and a single spin direction.

3.2 Cubic $LaMnO_3$ and Orthorhombic $LaMnO_3$. Next, we investigate the changes in the electronic properties associated with the transition to the low symmetry orthorhombic ground state in $LaMnO_3$. This comparison between cubic ferromagnetic, and orthorhombic antiferromagnetic $LaMnO_3$ will provide a benchmark with which to compare our later study of the transition from cubic to monoclinic ferromagnetic $BiMnO_3$. The structural change in going from the cubic to the orthorhombic phase is, to a first approximation, driven by La being too small for the 12-coordinate A site in the perovskite structure. Therefore, even at temperatures as high as 1000 K, there is a tilt of the MnO_6 octahedra around the pseudocubic [111] direction.[28] The second factor driving the structural change is the Jahn−Teller nature of Mn^{III} which favors distorted MnO_6 octahedra below a cooperative transition at $T_{JT} \approx 750$ K.[28] The Jahn−Teller distortion splits the previously degenerate e_g levels into a more stable, filled d_{z^2} and a less stable unfilled $d_{x^2-y^2}$. These factors combine to stabilize the A-type antiferromagnetic order[29,25] and the orthorhombic structure. The partial densities of states for the two $LaMnO_3$ structures are presented in Figure 5. The states have been scaled for a single spin direction and for the $LaMnO_3$ composition. Note that the Mn density of states is shown for a single up spin Mn atom; there is a corresponding down spin Mn atom with the oppositely polarized density of states related to the first by the antiferromagnetic symmetry. The first thing we

(28) Rodríguez-Carvajal, J.; Hennion, M.; Moussa, F.; Moudden, A. H.; Pinsard, L.; Revcolevschi, A. *Phys. Rev. B* **1997**, *57*, 3189.
(29) Wollan, E. O.; Koehler, W. C. *Phys. Rev.* **1955**, *100*, 545.

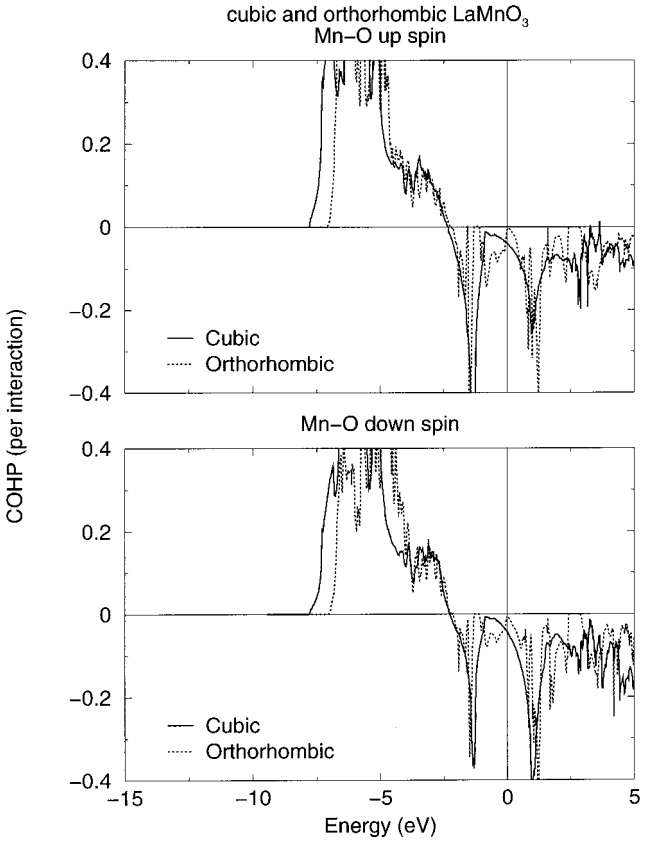

Figure 6. Crystal orbital Hamiltonian populations (COHPs) between Mn and O in cubic and orthorhombic $LaMnO_3$. The COHPs are scaled to a single MnO_6 octahedron.

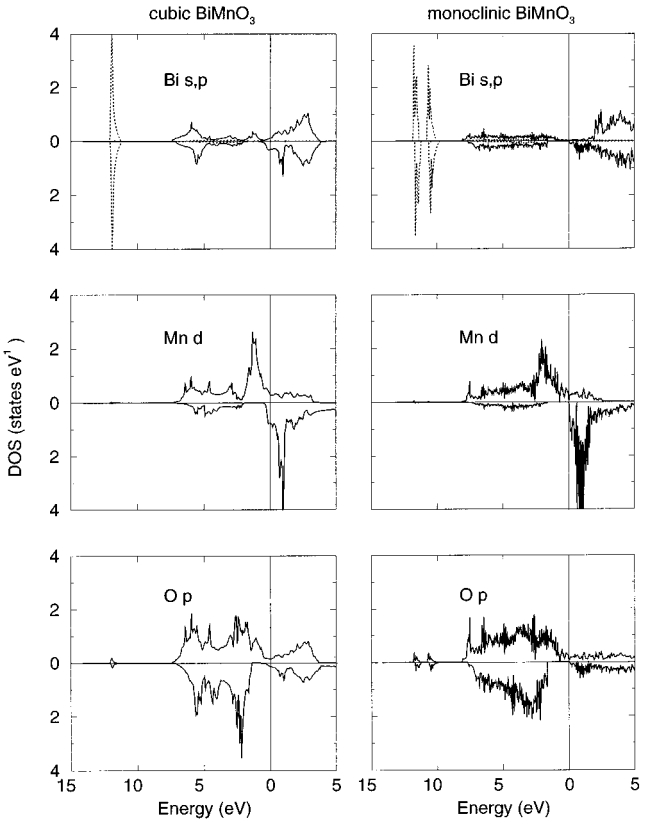

Figure 7. Projected DOS of cubic ferromagnetic $BiMnO_3$ and monoclinic ferromagnetic $BiMnO_3$. The DOS have been scaled to a single spin direction and to one $BiMnO_3$ formula unit.

notice is that the artificial density of La states below the Fermi energy which was present in the cubic structure is absent in the orthorhombic structure. This is because the La sphere in the orthorhombic phase has a much more realistic diameter, and the predominantly ionic bonding between La and O is more accurately reflected. In addition, the sharp features found in the Mn and O states in the cubic phase are now significantly smoother.

In the orthorhombic phase, the Jahn−Teller distortion results in the electronic configuration $t_{2g}^3 d_{z^2}^1 d_{x^2-y^2}^0$ which when spin polarized, allows a gap to open between $d_{z^2}^1(\uparrow)$ and $t_{2g}^0(\downarrow)$. Orthorhombic A-type $LaMnO_3$ is therefore a band antiferromagnetic insulator within the present computational scheme. We should point out that only when nonlocal exchange correlation potentials are invoked does such a gap open in these LMTO-ASA calculations. (The local spin density approximation (LSDA) fails to give a gap even in the ground-state orthorhombic structure). The downward shift in energy of the lower e_g peak can be seen by comparing the Mn DOSs in the cubic and orthorhombic structures. This downward shift contributes to the energy stabilization of the orthorhombic phase. There is only a slight difference in the widths and relative occupancies of the Mn and O bands on going from the cubic ferromagnetic to the orthorhombic antiferromagnetic $LaMnO_3$, suggesting minimal changes in the amount of Mn−O covalency between the two structures.

Such changes in the extent of Mn−O covalency are better visualized through examining the crystal orbital Hamiltonian populations (COHPs), which permit a quantitative demarcation of bonding (positive COHPs), nonbonding, and antibonding (negative COHPs) regimes along an energy axis. Figure 6 compares the Mn−O COHPs (per octahedron) in the two different spin directions of cubic and orthorhombic $LaMnO_3$. Note that while the gross features are similar, the COHPs reveal that the reduction in symmetry actually reduces the extent of the favorable bonding hybridization in orthorhombic $LaMnO_3$, pushing up the bottom of the bonding COHP by about 1 eV. The energy stabilization in Jahn−Teller distorted compounds comes largely from the almost rigid shift to lower energy of the occupied e_g orbital, rather than from an increase in energetically favorable hybridization.

3.3 Cubic $BiMnO_3$ and Monoclinic $BiMnO_3$. The combination of a small A atom (as in $LaMnO_3$) and the Jahn−Teller nature of Mn^{III} might lead us to anticipate that $BiMnO_3$ would crystallize in an orthorhombic structure similar to $LaMnO_3$. Instead, it crystallizes in a monoclinic structure that is unusual in its highly distorted off-centered MnO_6 octahedra as well as in Mn−O−Mn bond angles (ranging from 140° to 160°) that are significantly smaller than the ideal 180°.[9] Within the present LMTO scheme, a ferromagnetic state is obtained for monoclinic $BiMnO_3$ with an average magnetic moment of 4.0 μ_B per Mn, equal to the ideal spin-only value. In this rather complicated structure, there are many possible antiferromagnetic arrangements. We have performed a calculation for one of them, which has ferromagnetic layers stacked antiferromagnetically along the monoclinic *a* axis of the structure. The ferromagnet is stabilized by 27 meV over this particular antiferromagnetic arrangement suggesting

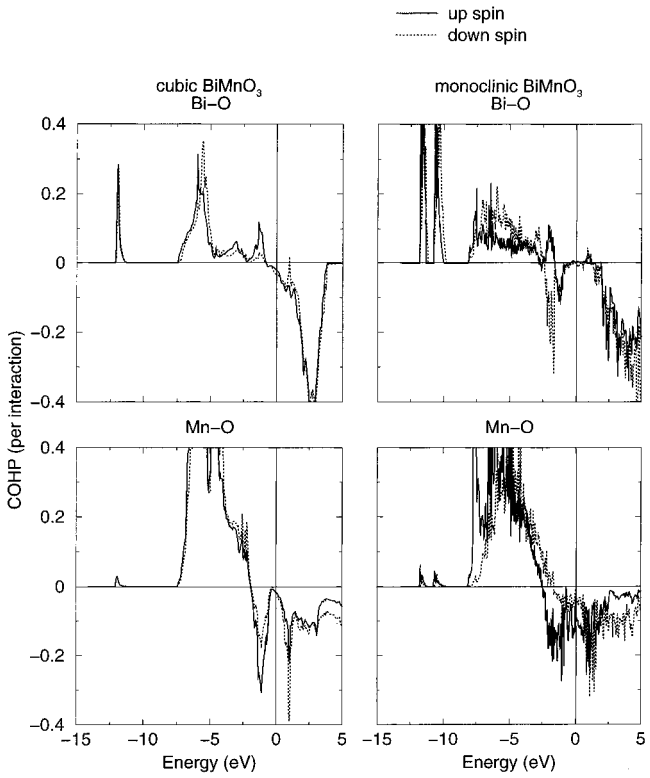

Figure 8. Various metal oxygen COHPs in cubic and monoclinic $BiMnO_3$. The Bi−O COHPs are scaled to 12 Bi−O interactions and the Mn−O COHPs are scaled to one octahedron (six interactions).

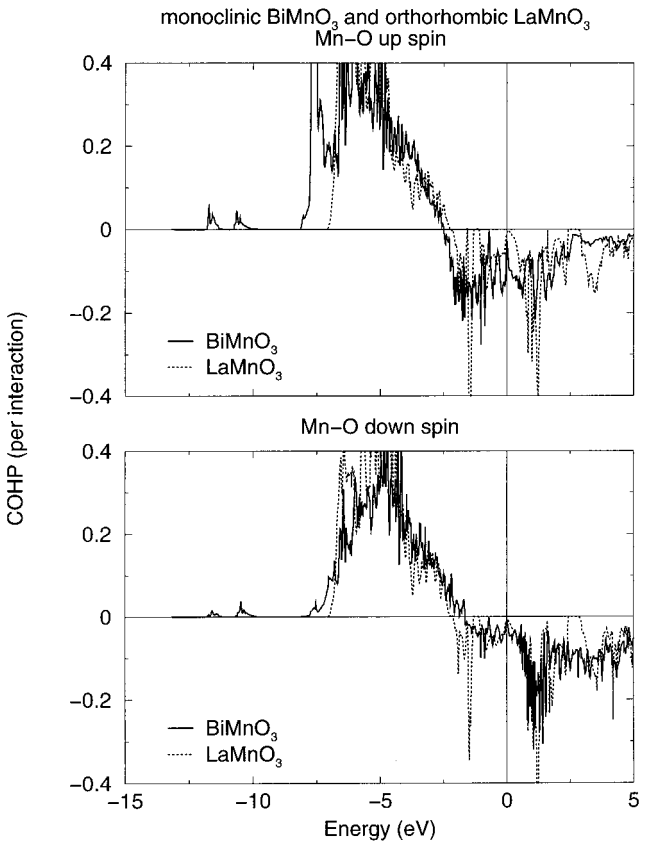

Figure 9. Comparison of the Mn−O COHPs (per octahedron) of orthorhombic $LaMnO_3$ and monoclinic $BiMnO_3$.

that a ferromagnetic ground state of $BiMnO_3$ is obtained within the present computational scheme.

Figure 7 compares the orbital resolved densities of states in ferromagnetic cubic and monoclinic $BiMnO_3$. There are two distinct Bi atoms in the monoclinic phase, and their lone pair $6s^2$ levels are separated. The Mn and O densities of states are similar, except that monoclinic $BiMnO_3$ is nearly gapped at the Fermi energy for the same reason that a gap appears in orthorhombic antiferromagnetic $LaMnO_3$.

The first notable feature is that the Mn and O bands are wider and shifted down in energy in the monoclinic phase as compared with the cubic phase. This indicates that the Mn−O hybridization increases as a result of the structural distortion, in sharp contrast to the covalency in $LaMnO_3$, which we observed to decrease with the structural distortion. Such an increase in hybridization has been observed previously in ferroelectric phase transitions in hexagonal manganites.[8] Ferroelectric behavior of the Mn−O octahedron is consistent with the recent structural data which reports an off-center distortion of the Mn within the oxygen octahedron.[9] However, such a noncentrosymmetric distortion is most unusual for a d^4 Jahn−Teller ion.

Additional important differences between the cubic and monoclinic phases appear in the Bi−O and Mn−O COHPs shown in Figure 8. First, the Bi−O COHP is more disperse in the monoclinic phase indicating Bi−O hybridization over a broader energy range. In particular, the COHP strength in the region of the Bi 6s states is increased significantly. This suggests greater mixing between the Bi 6s lone pair states and the oxygen states, which implies that the lobe shape of the lone pair in the monoclinic phase might be the result of mixing with oxygen (rather than Bi) p states. Although at variance with the traditional "text book" picture of lone pairs, such mixing of the ligand states with the cation 6s states has also been suggested recently for PbO.[12] Second, the Bi−O COHP shows some antibonding states just below E_F. When two closed-shell systems interact, one expects no net bonding between them. This means that all filled bonding states are compensated by filled antibonding states. The fact that in monoclinic $BiMnO_3$ (but not in the cubic compound) one finds antibonding states below the Fermi level implies that there is some closed-shell character to the distorted Bi in $BiMnO_3$. The closed-shell character arises from the localization of the lone pair $6s^2$ states into lobes which form shells that are effectively inert to bonding. The Mn−O COHPs display a slight broadening in the monoclinic phase because of the spread in the Mn−O bond distances. The difference in the Mn−O COHPs in the two spin directions is more marked in the monoclinic phase than it is in the cubic phase, with an increase in the up-spin bonding interaction and a decrease in the down-spin antibonding interaction.

3.4 Monoclinic $BiMnO_3$ and orthorhombic $LaMnO_3$. Finally, we compare the low-temperature phases of $BiMnO_3$ and $LaMnO_3$, anticipating that differences in the electronic structures of these two compounds will arise from the Bi $6s^2$ lone pair and the off-centered MnO_6 octahedra in $BiMnO_3$.

Figure 9 displays the Mn−O COHPs of the two low symmetry phases in the two spin directions. It is striking that there is significant stabilization of the Mn−O COHP in the Bi compound with the bottom of

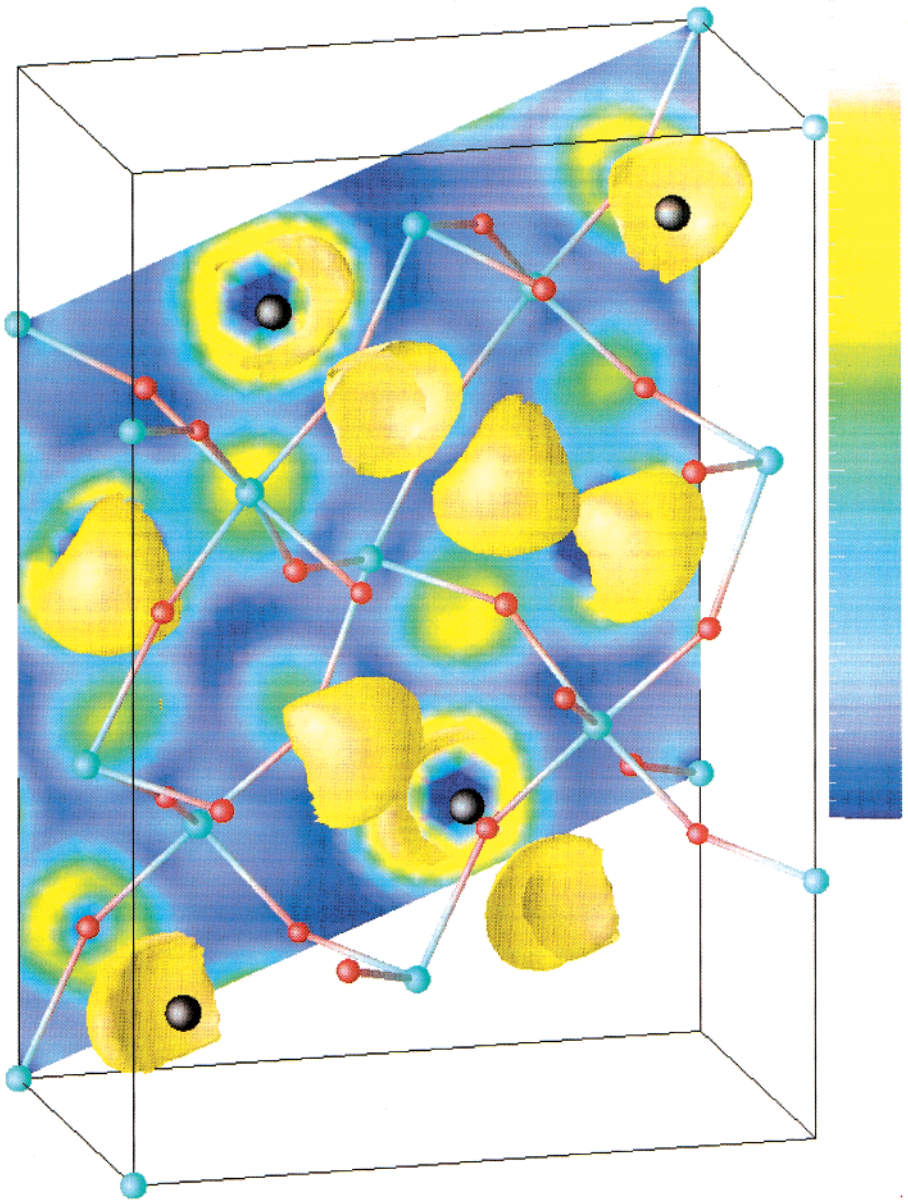

Figure 10. Isosurface (at a value of 0.75) of the valence ELF of monoclinic $BiMnO_3$ projected within a unit cell. Blue corresponds to almost no electron localization, and white corresponds to complete localization. The projection on one of the cell faces is of the valence ELF, color coded as in the bar by the side of the figure. The view of the crystal is nearly down the *b* axis as in Figure 1.

the spin up COHP being about 1 eV below the bottom of the spin up COHP in the La compound. This arises because the off-center distortion in $BiMnO_3$ results in an Mn−O bond that is as short as 1.78 Å,[9] whereas the shortest Mn−O distances in orthorhombic $LaMnO_3$ are of the order of 1.9 Å (ref 24).

In Figure 10, we again display the structure of monoclinic $BiMnO_3$ with black spheres representing Bi and cyan spheres (bonded to red O) representing Mn. In the space of the unit cell, we have plotted isosurfaces of a constant valence-only ELF of 0.75. The projection is a perspective view down an axis close to the *b* axis of the unit cell. The visible regions in the isosurface correspond to the lobe-like Bi lone pair that is permitted by the distorted geometry of the monoclinic structure to adopt a traditional lone-pair geometry. Note that our DOS calculations confirm that this lobe is indeed composed largely of the Bi $6s^2$ lone pair, with some oxygen p and Bi p admixture, but is certainly not composed primarily of Bi p states. The transformation from a nearly spherical lone pair in the cubic phase to a lobe-like lone pair in the monoclinic phase is perhaps the driving force for some of the structural distortions in this system. Following the terminology of Silvi and Savin,[22] the lone pair in the cubic phase forms a domain of localization that is reducible and therefore unstable while in the orthorhombic phase, the domain of localization (the lobe) is irreducible, containing a single attractor.

Conclusions and Future Work

In conclusion, our calculations indicate that the lone pair on the Bi ion in $BiMnO_3$ is stereochemically active and is the primary driving force behind the highly distorted low temperature monoclinic structure observed in this material. We also suggest that the occurrence of ferroelectricity is likely in $BiMnO_3$, and, if confirmed experimentally, will be a consequence of the Bi lone pair. Our calculations indicate that the

localized lone pair in the distorted structure is not composed only of the expected Bi 6s and 6p states, but also has some contribution from the 2p states on the oxygen ligands. [Note that an increase in covalent bonding between oxygen and cation states on distortion is also observed in prototypical ferroelectric perovskite oxides such as $BaTiO_3$. However in the conventional ferroelectrics this increased hybridization occurs primarily between the O 2p electrons and empty states on the small (B) cation.] The degree of mixing between the Bi states and the ligand states is clearly strongly dependent on the nature of the ligand, and so the choice of anion might be an important variable in the design of Bi-based ferroelectric materials.

We also see that the Mn−O covalency is strong and that the electronic structure around the Mn ion is similar in $BiMnO_3$ and in antiferromagnetic, nonferroelectric $LaMnO_3$. Therefore, we conclude that the different magnetic properties and different distortions around the Mn−O octahedra are also the result of the structural distortions driven by the stereochemically active Bi ion. We are currently embarking on a study of $BiAlO_3$, in which the B cation does not have d electrons, to isolate the contribution of the Bi ion from that of the magnetic ion.

Acknowledgment. We thank Umesh Waghmare and J. Gopalakrishnan for useful suggestions and encouragement, and the group of Professor O. K. Andersen for providing us the LMTO codes. N.A.H. is supported by National Science Foundation's Division of Materials Research under grant number DMR 9973076 and thanks the Jawaharlal Nehru Center for Advanced Scientific Research for their hospitality during the recent sabbatical leave when this work was initiated. R.S. is supported by the Council of Scientific and Industrial Research, India.

CM010090M